International Journal of Solids and Structures 58 (2015) 233–246

Contents lists available at ScienceDirect

International Journal of Solids and Structures

journal homepage: www.elsevier.com/locate/ijsolstr

Modeling of multi-strand wire ropes subjected to axial tension and torsion loads

L. Xiang [a], H.Y. Wang [a], Y. Chen [a], Y.J. Guan [a], Y.L. Wang [b], L.H. Dai [a,*]

[a] State Key Laboratory of Nonlinear Mechanics, Institute of Mechanics, Chinese Academy of Sciences, Beijing 100190, China
[b] Naval Armament Academy, Beijing 100161, China

ARTICLE INFO

Article history:
Received 24 September 2014
Received in revised form 25 November 2014
Available online 17 January 2015

Keywords:
Multi-strand wire rope
Double-helix
Local deformation and stress
Curvature and twist
Thin rod theory

ABSTRACT

A new model characterizing the response of a multi-strand wire rope subjected to axial tension and axial torque is presented in this paper. Apart from most of previous approaches which deal with a straight wire strand, the present model fully considers the double-helix structure in multi-strand configuration. To be further, a new method to compute local deformation parameters (two curvatures and a twist defined by Love, 1944) of each wire is introduced. The proposed model well predicts the global stiffness of the rope. It is found that different friction states between adjacent wires can lead to quite a different distribution of local bending and torsion deformation of double-helix wire. The variations of stresses in double-helix wires along the rope axis are analyzed and the results show that torsion stress of a double-helix wire can be neglected when the rope is subjected to axial tension (axial torsion is restrained). The present model provides a new way to estimate the local deformation and stresses at the wire level, which sheds new insight into the understanding of the fatigue and failure behavior of the wire rope.

1. Introduction

Helical structures like wire ropes have been widely used in elevator lifting, suspension bridges, aerial rope ways, mine hoists, etc. Due to their capacity to support large tensile load with relatively small bending or torsion stiffness, wire ropes are usually employed as load transmission elements especially when they have to be bent over sheaves or drums. During past decades, extensive theoretical and experimental works have been made to characterize the mechanical behavior of wire ropes. A systematical work of these was presented by Feyrer (2006). Great concern has been paid to the global response of the wire ropes, such as the tensile and bending stiffness, and also the local deformation of individual wire, which are critically related to the fatigue and damage behavior of the wire ropes. The degree of damage is closely associated with the geometrical and spatial configuration of the wires as well as their positions within the rope (Lee, 1991).

A simple wire rope can just be a multi-layer single straight strand, in which all spiral wires are configured as *single-helix*. However, complex wire ropes are constructed from several strands that are wound around a core. The center wire of a wound strand is still *single-helix* while other wires in the strand are configured as *double-helix*. In general, two types of lay construction are used in complex wire ropes: regular lay and lang lay. In regular lay construction, the lay direction of the wires within the wound strand is opposite to the spiral direction of the strands around the core. In lang lay construction, the two directions are the same.

Currently, a majority of mathematical models have been applied to a single, straight strand to study the mechanical property of wire ropes. A review of these models was given by Cardou and Jolicoeur (1997). Among them, the fiber model is the simplest one, which assumes a fibrous response of each wire and ignores its bending and torsion rigidity. This model was introduced by Hruska (1952a,b) and later extended by Knapp (1979) and Lanteigne (1985). However, the bending and torsion stiffness are not actually negligible for the wires. Hence, some new models considering bending and torsion effects are needed to be developed.

Costello and Philips (1976) presented a thin rod model, based on the nonlinear equations of equilibrium of curved rods (Love, 1944). This model considers the bending and torsion stiffness of the wires and ignores the friction force, which was recently extended by Kumar and Cochran (1987) to a linearized and closed-form expression for the global stiffness of the rope. LeClair and Costello (1988) discussed the friction effects of strands subjected to bending load. Utting and Jones (1987a,b) have extended the Costello's analysis to include wire flattening (contact deformation) and friction effects. The results show that these phenomena

* Corresponding author. Tel.: +86 10 82543958; fax: +86 10 82543977.
E-mail address: lhdai@lnm.imech.ac.cn (L.H. Dai).

http://dx.doi.org/10.1016/j.ijsolstr.2015.01.007
0020-7683/

have little effect on estimation of the global rope response. Jolicoeur and Cardou (1991) compared the mechanical response of a single strand rope predicted by Costello's thin rod model with that estimated by fiber model (Hruska, 1952a,b). It was found that the fiber model is not appropriate when twisting moment and angle have to be taken into account and the thin rod model shows a good prediction of cable stiffness with experimental results obtained by Utting and Jones (1987b).

In contrast to the thin rod models, a semi-continuous model (so-called orthotropic sheet model) was introduced by Hobbs and Raoof (1982) and described in detail by Raoof (1983), in which each layer of twisted wire is modeled as an orthotropic complete cylinder. The same homogenization was taken by Blouin and Cardou (1989) to develop another semi-continuous model. Jolicoeur (1997) reported a comparative study of these models. He found that the former cylinder model is simpler and would be preferred for tension or torsion loads, but fails to capture the range of bending stiffness, so the latter semi-continuous model should be used if bending will occur (Spak et al., 2013). Raoof and Kraincanic (1994) compared the semi-continuous models with thin rod models for cable analysis and found that thin rod theory was more reliable for small diameter wire strand, while semi-continuous models would be advantageous for cables made of a large number of wires.

All the above models are only treating a single-helix wire strand. However, most wire ropes in practical use have a complex multi-strand cross-section in which most wires are configured double-helix (Argatov, 2011). Lee (1991) discussed in detail the geometrical property of single-helix and double-helix wires and pointed out that there existed many differences between them. Recently, a concise mathematical model was introduced by Stanova et al. (2011a) for both the single-helix and the double-helix configurations in the form of parametric equations. Their method presents high efficiency in building the finite element model of wire ropes and the numerical results of a multi-layered strand under tension tests were given, which agree well with experimental data (Stanova et al., 2011b). Inagaki et al. (2007) analyzed the mechanical behavior of second order helical structure in electrical cables, whose attention was paid to the response of cables subjected to bending load.

Velinsky (1981) and Velinsky et al. (1984) extended Costello's model to a complex multi-strand wire rope and treated a wound strand as being a single-helix wire in a straight strand. They first calculated the tension, torsion and bending stiffness of a straight strand, and then used the parameters to get the resultant tension and torque of the strand when it is wrapped around the central core. As a consequence, this homogenization may produce some difficulty in obtaining the local response of double-helix wires completely. Velinsky's approach was generalized by Phillips and Costello (1985) for wire rope with an independent wire rope core (IWRC) and summarized in the book *Theory of Wire Rope* (Costello, 1990). Ghoreishi et al. (2007a,b) introduced a similar homogenization procedure to get the mechanical character of a 1 + 6 synthetic fiber rope.

The double-helix configuration was first fully considered by Elata et al. (2004) for simulating the mechanical behavior of a wire rope with IWRC under axial loads. They took two different kinematics of wires: *locked rope-level sieves* that emulate infinite friction between adjacent wires and *unlocked rope-level sieves* that emulate a well lubricated rope. In the first kinematics the axial strain varies periodically along the centerline of the double-helix wires, while it is uniform in the second kinematics. Fiber assumption was retaken to simplify the analysis procedure, and the wires are subjected to load on their lateral surface, applied by adjacent wires. Therefore, the accuracy of this model improves when the number of wires in the wire rope increases (Ghoreishi et al., 2007c).

Usabiaga and Pagalday (2008) developed another model for double-helix cables, but did not take Poisson effect into consideration. The model is based on the work of Ashkenazi et al. (2003) and the general thin rod theory (Love, 1944), and assumes that the wires are un-lubricated to prevent relative movements between adjacent wires. However, instead of attaching the material points of each wire section to the central wire of the rope as Ashkenazi et al. (2003), Usabiaga and Pagalday (2008) attached those points to the central wire of the wound strand. The local curvatures and twist results along double-helix wires of the two kinematics showed great difference. Besides, a detailed and rigorous description of the procedure is employed to compute Love's (1944) kinematic parameters by Usabiaga and Pagalday (2008).

In this article, we focus our attention on the double-helix configuration and take a typical 7×7 wire rope (i.e. IWRC, see Fig. 1) into consideration. Instead of adding additional kinematics to the wires, a new method to calculate the local curvatures and twist of the wires is proposed, based on the general thin rod theory of Love (1944) and frictionless hypothesis between adjacent wires. Some effective procedures to get the axial strain along the wires are also introduced. The global response of the rope and the local deformation and stresses of individual wires are analyzed and the results are compared with those of the popular homogenized model of Costello (1990) and other models for complex multi-strand wire ropes.

2. Wire centerline descriptions

A Cartesian coordinate system $\{\boldsymbol{e}_X, \boldsymbol{e}_Y, \boldsymbol{e}_Z\}$ is used to describe the structure of the rope where the rope axis is along the $\boldsymbol{e}_z$ direction. In the initial configuration, a generic centerline of a single-helix wire is given by the following parametric equation:

$$x_{s0} = r_{s0}\cos\theta_s \tag{1a}$$

$$y_{s0} = r_{s0}\sin\theta_s \tag{1b}$$

$$z_{s0} = r_{s0}\tan\alpha_{s0}\theta \tag{1c}$$

where r_{s0} is the laying radius of the single-helix, α_{s0} is the single-helix laying angle, θ_s represents the angular position around the rope axis $\boldsymbol{e}_Z$ relative to $\boldsymbol{e}_X$ (Fig. 2) and $\theta_s = \theta + \theta_{s0}$. θ is a free parameter representing the angle of the centerline spiral around the axis of the rope and θ_{s0} is the single-helix phase angle indicating the wire position relative to $\boldsymbol{e}_X$ when $z_{s0} = 0$ (i.e. when $\theta = 0$), that is $\theta_{s0} = \theta_{s(z_{s0}=0)}$.

A generic description of the centerline of a double-helix wire in its initial configuration is derived by Usabiaga and Pagalday (2008):

$$x_{w0} = x_{s0} - r_{w0}\cos\theta_w\cos\theta_s + r_{w0}\sin\theta_w\sin\theta_s\sin\alpha_{s0} \tag{2a}$$

$$y_{w0} = y_{s0} - r_{w0}\cos\theta_w\sin\theta_s - r_{w0}\sin\theta_w\cos\theta_s\sin\alpha_{s0} \tag{2b}$$

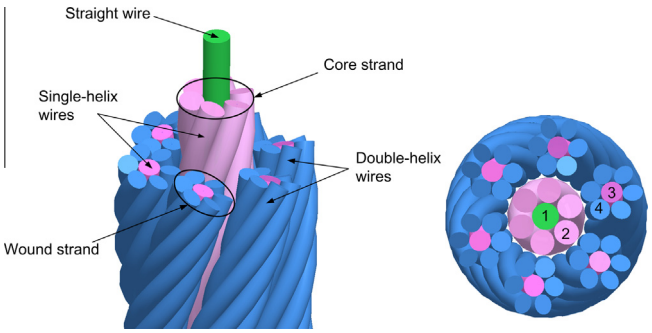

Fig. 1. A 7×7 wire rope with cross section.

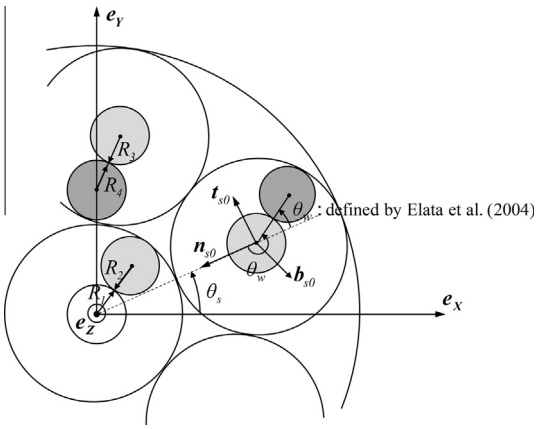

Fig. 2. Geometric features of the wire rope structure.

$$z_{w0} = z_{s0} + r_{w0}\sin\theta_w\cos\alpha_{s0} \tag{2c}$$

where r_{w0} is the spiral radius of the double-helix wire laying around its corresponding single-helix wire, θ_w represents the angular position around the Frenet–Serret vector $\boldsymbol{t}_{s0}$ relative to $\boldsymbol{n}_{s0}$ (Fig. 2) and $\theta_w = m\theta + \theta_{w0}$. $\theta_{w0}$is the double-helix phase angle denoting the wire position relative to $\boldsymbol{n}_{s0}$ when $\theta = 0$, that is $\theta_{w0} = \theta_{w(\theta=0)}$, and m is a construction parameter which is related to the geometrical property of the rope, given as

$$m = \frac{r_{s0}}{r_{w0}}\frac{1}{\tan\beta_{w0}\cos\alpha_{s0}} \tag{3}$$

where β_{w0} is the double-helix laying angle.

One may notice that Eqs (2a)–(2c) have differences in +/− signs with the equations developed by Elata et al. (2004). This is due to the different definition of θ_w. As explained previously, θ_w represents the angular position around $\boldsymbol{t}_{s0}$ relative to $\boldsymbol{n}_{s0}$ in this paper, while θ_w defined by Elata et al. (2004) represents the angular position around $\boldsymbol{t}_{s0}$ relative to $-\boldsymbol{n}_{s0}$ (Fig. 2).

In the following statement, the subscript 's' and 'w' represent the single-helix and the double-helix respectively. Without losing generality, we take the wire with $\theta_{s0} = 0$ and $\theta_{w0} = 0$ for a typical study, unless specially noted.

When the rope is subjected to axial load, the global deformation parameters are the rope tensile strain ε_t and the rope torsion k_t:

$$\varepsilon_t = \frac{L - L_0}{L_0} \tag{4a}$$

$$k_t = \frac{\Delta\phi}{L_0} \tag{4b}$$

where L_0 and L are the rope lengths in the undeformed and deformed configuration respectively and $\Delta\phi$ is the relative torsion angle between the two ends of the rope.

Elata et al. (2004) gave the location along the stressed centerline of a double-helix wire along with the global deformation of the rope:

$$x_w = \sqrt{x_{w0}^2 + y_{w0}^2}\cos\left[\tan^{-1}\left(\frac{y_{w0}}{x_{w0}}\right) + k_t z_{w0}\right] \tag{5a}$$

$$y_w = \sqrt{x_{w0}^2 + y_{w0}^2}\sin\left[\tan^{-1}\left(\frac{y_{w0}}{x_{w0}}\right) + k_t z_{w0}\right] \tag{5b}$$

$$z_w = z_{w0}(1 + \varepsilon_t) \tag{5c}$$

However, this expression exhibits an arctangent function so that the future derivation (like differential operation) with these equations may have some difficulty. It can be improved as:

$$x_w = x_{w0}\cos(k_t z_{w0}) - y_{w0}\sin(k_t z_{w0}) \tag{6a}$$

$$y_w = x_{w0}\sin(k_t z_{w0}) + y_{w0}\cos(k_t z_{w0}) \tag{6b}$$

$$z_w = z_{w0}(1 + \varepsilon_t) \tag{6c}$$

The location along the stressed centerline of a single-helix wire can be expressed by similar equations, which are also given by Usabiaga and Pagalday (2008):

$$x_s = r_{s0}\cos(\theta_s + k_t z_{s0}) \tag{7a}$$

$$y_s = r_{s0}\sin(\theta_s + k_t z_{s0}) \tag{7b}$$

$$z_s = z_{s0}(1 + \varepsilon_t) \tag{7c}$$

Radial contraction due to Poisson effect in the wire diameter is neglected in all of the above equations.

3. Local deformation along a wire

Ignoring the effect of contact deformation, the kinematics of a particular wire is fully defined by four parameters: the axial strain ξ, two curvatures κ and κ' and the twist τ. In this section, we will give a detailed analysis of these local deformation parameters by introducing some mathematical skills and the thin rod theory of Love (1944).

3.1. The Frenet–Serret frames

The centerline of any wire in a rope is a three-dimensional space curve. It is convenient to use the well-known Frenet–Serret local axes $\{\boldsymbol{t}_0, \boldsymbol{n}_0, \boldsymbol{b}_0\}$ (undeformed configuration) and $\{\boldsymbol{t}, \boldsymbol{n}, \boldsymbol{b}\}$ (deformed configuration) at each point of the wire trajectory to enable a better understanding of its local deformation. Here $\boldsymbol{t}$ is the tangent unit vector, $\boldsymbol{n}$ is the principal normal and $\boldsymbol{b}$ is the binormal vector. $\boldsymbol{t}_0$ and $\boldsymbol{t}$ are always along the tangential direction of the centerline at any point (Fig. 3).

According to the Frenet–Serret frame, the curvature of a space curve can be calculated by virtue of (Lee, 1991)

$$\kappa_F = \sqrt{\frac{(\dot{y}\ddot{z} - \dot{z}\ddot{y})^2 + (\dot{z}\ddot{x} - \dot{x}\ddot{z})^2 + (\dot{x}\ddot{y} - \dot{y}\ddot{x})^2}{(\dot{x}^2 + \dot{y}^2 + \dot{z}^2)^3}} \tag{8}$$

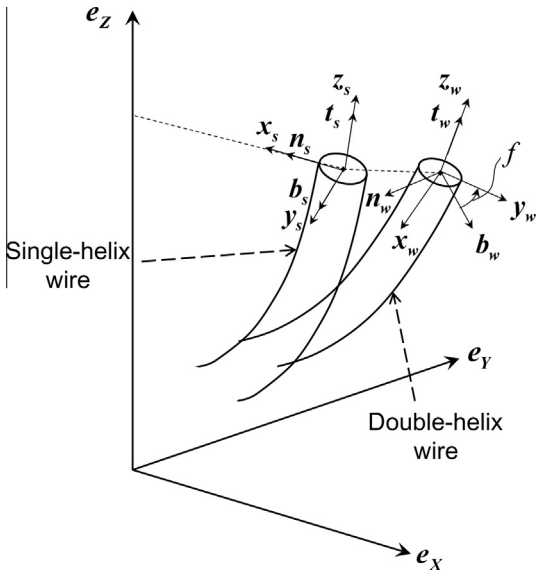

Fig. 3. Local coordinate systems along wires.

and the torsion of a space curve can be computed by

$$\tau_F = \frac{\begin{vmatrix} \dot{x} & \dot{y} & \dot{z} \\ \ddot{x} & \ddot{y} & \ddot{z} \\ \dddot{x} & \dddot{y} & \dddot{z} \end{vmatrix}}{(\dot{y}\ddot{z} - \dot{z}\ddot{y})^2 + (\dot{z}\ddot{x} - \dot{x}\ddot{z})^2 + (\dot{x}\ddot{y} - \dot{y}\ddot{x})^2} \tag{9}$$

It should be noted that the principal normal vectors $\boldsymbol{n}_{s0}$ (derived from Eq. (1)) and $\boldsymbol{n}_s$ (derived from Eq. (7)) of a single-helix centerline always point to the axis of the rope (Fig. 3). However, one can verify that the principal normal vectors $\boldsymbol{n}_{w0}$ and $\boldsymbol{n}_w$ of a double-helix centerline do not always lay in the direction to its corresponding single-helix centerline but vary periodically in the neighborhood region (Fig. 3).

3.2. The principal torsion–flexure axes

In order to describe the general deformation of a thin rod, Love (1944) introduced an orthonormal local frame $\{\boldsymbol{x}, \boldsymbol{y}, \boldsymbol{z}\}$ called *principal torsion-flexure axes*, which was defined on the centerline for every cross section of the rod. The third vector $\boldsymbol{z}$ of these frames is always along the tangential direction of the centerline at any point, so the difference between these axes and the Frenet–Serret axes is that they generate an angle f in the $(\boldsymbol{x}, \boldsymbol{y})$ or $(\boldsymbol{n}, \boldsymbol{b})$ plane (Fig. 3).

In the initial configuration, the selection of *principal torsion–flexure axes* has some arbitrariness that the normal and binormal vectors just need to be perpendicular to each other and constitute an orthonormal frame with the tangent vector. When the rod is subjected to external load, the initial *principal torsion–flexure axes* should stick to the cross section of the rod and move along with the centerline, which means that material points in the direction of the initial normal vector $\boldsymbol{x}_0$ should lay in the direction of the normal vector $\boldsymbol{x}$ after deformation. It indicates a one-to-one corresponding relationship between the material points in the undeformed and deformed state.

The thin rod theory of Love (1944) introduced two curvatures κ and κ' and a twist τ to represent the local deformation of the rod. When the *principal torsion–flexure axes* are fully determined, they can be calculated by

$$\kappa = l_3 \frac{dl_2}{ds} + m_3 \frac{dm_2}{ds} + n_3 \frac{dn_2}{ds} \tag{10a}$$

$$\kappa' = l_1 \frac{dl_3}{ds} + m_1 \frac{dm_3}{ds} + n_1 \frac{dn_3}{ds} \tag{10b}$$

$$\tau = l_2 \frac{dl_1}{ds} + m_2 \frac{dm_1}{ds} + n_2 \frac{dn_1}{ds} \tag{10c}$$

where, for example, l_1, m_1, n_1 are the direction cosines of the axis $\boldsymbol{x}$ referred to the fixed axes.

In fact, another method to compute these kinematic parameters is also given by Love (1944):

$$\kappa = -\kappa_F \cos f_L \tag{11a}$$

$$\kappa' = \kappa_F \sin f_L \tag{11b}$$

$$\tau = \tau_F + \frac{df_L}{ds} \tag{11c}$$

where s is the arc parameter along the centerline and $\frac{1}{2}\pi - f_L$ is the angle between the principal plane $(\boldsymbol{x}, \boldsymbol{z})$ of the rod and the principal normal vector $\boldsymbol{n}$ of the strained centerline.

As we have explained, f denotes the angle between $\boldsymbol{n}$ of the Frenet–Serret axes and $\boldsymbol{x}$ of the *principal torsion–flexure axes*, so $\frac{1}{2}\pi - f_L = -f$. Then more concise equations to compute κ, κ' and τ are:

$$\kappa = \kappa_F \sin f \tag{12a}$$

$$\kappa' = \kappa_F \cos f \tag{12b}$$

$$\tau = \tau_F + \frac{df}{ds} \tag{12c}$$

Eq. (12) is important to determine the local deformation of double-helix wires in this paper and it can be seen that key problem to determine the *principal torsion–flexure axes* has came down to getting the value of f.

3.3. Curvatures and twist

Fig. 4 illustrates the most general case of loading on a wire. On a given cross section, it has three components of force: the two components of shear force N and N' in $\boldsymbol{x}$ and $\boldsymbol{y}$ directions respectively, and the tension T in $\boldsymbol{z}$ direction. It also has three components of moment: the two components of bending moment G and G' in $\boldsymbol{x}$ and $\boldsymbol{y}$ directions respectively, and the torsion moment H in $\boldsymbol{z}$ direction. There are also distributed forces, such as contact forces, and distributed moments that act on the outer surface of the wire. These distributed forces and moments are denoted by X, Y and Z and K, K' and Θ in $\boldsymbol{x}$, $\boldsymbol{y}$ and $\boldsymbol{z}$ directions, respectively.

The thin rod theory of Love (1944) gives the following force and moment balance equations:

$$\frac{dN}{ds} - N'\tau + T\kappa' + X = 0 \tag{13a}$$

$$\frac{dN'}{ds} - T\kappa + N\tau + Y = 0 \tag{13b}$$

$$\frac{dT}{ds} - N\kappa' + N'\kappa + Z = 0 \tag{13c}$$

$$\frac{dG}{ds} - G'\tau + H\kappa' - N' + K = 0 \tag{13d}$$

$$\frac{dG'}{ds} - H\kappa + G\tau + N + K' = 0 \tag{13e}$$

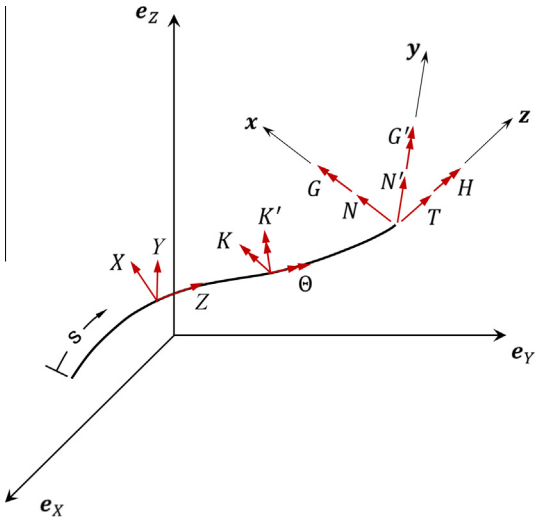

Fig. 4. Forces and moments acting on a wire (after Costello, 1990).

$$\frac{dH}{ds} - G\kappa' + G'\kappa - \Theta = 0 \tag{13f}$$

The bending and torsion moments of a wire cross section can be calculated from:

$$G = EI(\kappa - \kappa_0) \tag{14a}$$

$$G' = EI(\kappa' - \kappa_0') \tag{14b}$$

$$H = \mu J(\tau - \tau_0) \tag{14c}$$

Here, EI and μJ represent the bending and torsion stiffness, respectively. E is Young's modulus of the wire and μ is the shear modulus. In the case of a wire of circular cross-section with radius R, we have

$$EI = \frac{\pi}{4}ER^4, \quad \mu J = \frac{\pi ER^4}{4(1+\nu)} \tag{15}$$

It is necessary to establish the *principal torsion–flexure axes* of a wire before and after deformation. Usually we make the axes equivalent to the Frenet–Serret axes in the initial configuration to simplify the computation, i.e. $f_0 = 0$ at each point of wire centerline. In this case, we can get from Eq. (12):

$$\kappa_0 = 0, \quad \kappa_0' = \kappa_{F0}, \quad \tau_0 = \tau_{F0} \tag{16}$$

An additional assumption, $\Theta = 0$, is made for two reasons: first, the friction between adjacent wires is neglected. Secondly, the direction of contact force points to the center of every wire cross section, so it does not cause the torsional effect. Then we substitute Eqs. (12), (15) and (16) into Eq. (14) and get

$$G = \frac{\pi}{4}ER^4\kappa_F \sin f \tag{17a}$$

$$G' = \frac{\pi}{4}ER^4(\kappa_F \cos f - \kappa_{F0}) \tag{17b}$$

$$H = \frac{\pi ER^4}{4(1+\nu)}\left(\tau_F + \frac{df}{ds} - \tau_{F0}\right) \tag{17c}$$

Taking Eqs. (12) and (17) into Eq. (13f) and assuming $\Theta = 0$, we obtain an equation for the angle f:

$$\frac{d(\tau_F - \tau_{F0})}{ds} + \frac{d^2 f}{ds^2} = (1+\nu)\kappa_F\kappa_{F0}\sin f \tag{18}$$

From the above equation, f can be determined and then the response of the wires can be described by κ, κ' and τ via Eq. (12).

For single-helix wires, the solution of Eq. (18) is quite simple, that is, f is still equal to zero after deformation as τ_{F0}, τ_F, κ_{F0} and κ_F derived from centerline descriptions of Eqs. (1) and (7) are all constants. This analysis is the same as that of Costello (1990) for single-helix wires. Then the variations of curvatures and twist of the wires can be derived as:

$$\Delta\kappa = \kappa - \kappa_0 = 0 \tag{19a}$$

$$\Delta\kappa' = \kappa' - \kappa_0' = \frac{\cos^2\alpha_s}{r_s} - \frac{\cos^2\alpha_{s0}}{r_{s0}} \tag{19b}$$

$$\Delta\tau = \tau - \tau_0 = \frac{\sin\alpha_s\cos\alpha_s}{r_s} - \frac{\sin\alpha_{s0}\cos\alpha_{s0}}{r_{s0}} \tag{19c}$$

As for double-helix wires, the situation is more complex because τ_{F0}, τ_F, κ_{F0} and κ_F do not keep constant but vary periodically along the wire centerline, which leads to a periodical variation of f. Therefore, we consider one period to save computation cost. The finite difference method is introduced to solve Eq. (18). It is transformed into

$$\left(\frac{d(\tau_F - \tau_{F0})}{ds}\right)_n + \frac{f_{n+1} - 2f_n + f_{n-1}}{(\Delta s)_n^2} = (1+\nu)(\kappa_F)_n(\kappa_{F0})_n \sin f_n \tag{20}$$

Here, the arc length of one period is divided into n_c segments and $n = 1,2,\ldots,n_c - 1$, which leads to a group of $n_c - 1$ simultaneous equations. Generally we take $n_c > 1000$ to ensure the computational accuracy. Δs is the length of one segment and given by

$$\Delta s = \left(\dot{x}_w^2 + \dot{y}_w^2 + \dot{z}_w^2\right)^{1/2}\Delta\theta \tag{21}$$

If we sketch a figure in which a variable varies with θ and take a boundary point of a period coincided with the origin point of the coordinates, τ_{F0}, τ_F, κ_{F0} and κ_F behave just like an even function (examples are given later in Figs. 8 and 9), so f can exactly meet Eq. (18) if it varies as an odd function. Thus the boundary condition can be reasonably chosen as: $f_n = 0$ when $n = 0$ and $n = n_c$. This condition (i.e. f equals zero at the boundary points of a period) can also be obtained from the kinematics assumption made by Usabiaga and Pagalday (2008) if we calculate κ, κ' and τ based upon Eq. (12).

The presented procedure is implemented with Matlab software, which helps to solve the nonlinear equation group gathered from Eq. (20). When the value of f in one period is known, it can be easily expanded to the whole points along the rope length.

3.4. Axial strain along a wire

Planar view of a double-helix centerline and its corresponding single-helix centerline in a wound strand is shown in Fig. 5. Let l_{s0} and h_{s0} be the initial circumferential length and the initial height of the single-helix centerline, respectively. We can easily get the following relations:

$$l_{s0} = r_{s0}\theta \tag{22}$$

$$h_{s0} = r_{s0}\theta\tan\alpha_{s0} \tag{23}$$

where $r_{s0} = R_1 + 2R_2 + 2R_4 + R_3$ if we suppose that the wires of different layers just contact with each other in the unloaded state.

As described by Eq. (7), the centerline of a single-helix wire deforms with the global deformation ε_t and k_t. l_s and h_s are the circumferential length and the height of the single-helix centerline after deformation, respectively. Ignoring the Poisson effect, we can get:

$$l_s = r_{s0}(\theta + k_t h_{s0}) \tag{24}$$

$$h_s = h_{s0}(1 + \varepsilon_t) \tag{25}$$

In frictionless condition, the axial strain along a wire is uniform and it can be directly computed for a single-helix wire by means of:

$$\xi_3 = \frac{\sqrt{(h_s)^2 + (l_s)^2}}{\sqrt{(h_{s0})^2 + (l_{s0})^2}} - 1 \tag{26}$$

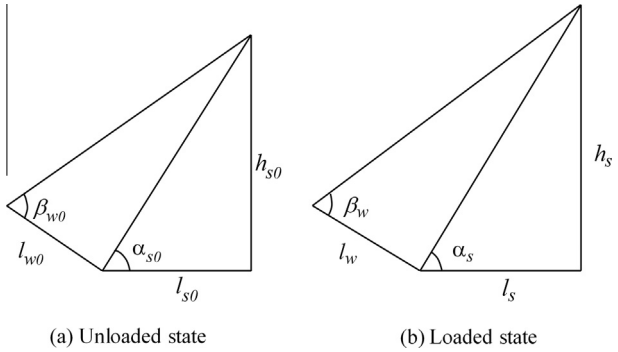

(a) Unloaded state (b) Loaded state

Fig. 5. Planar view of a double-helix centerline and its corresponding single-helix centerline.

Table 1
Main rope geometric parameters considered in this study.

Parameter	Value
R_1 (mm)	1.97
R_2 (mm)	1.865
R_3 (mm)	1.6
R_4 (mm)	1.5
$\alpha_{s0,2}$ (°)	71.01
$\alpha_{s0,3}$ (°)	71.46
$\beta_{w0,4}$ (°)	74.45

Then the curvature variation $\Delta\kappa_3'$ and the twist variation $\Delta\tau_3$ of the wire can be obtained from Eq. (19).

As for double-helix wires, let l_{w0} be the initial circumferential length of the double-helix centerline and

$$l_{w0} = r_{w0}\theta_w = \sqrt{(h_{s0})^2 + (l_{s0})^2} \Big/ \tan\beta_{w0} \tag{27}$$

where $r_{w0} = R_3 + R_4$.

In the loaded state, the double-helix centerline deforms along with its corresponding single-helix centerline. So the circumferential length of the double-helix centerline after deformation is

$$l_w = r_{w0}(\theta_w \pm r_{w0}\theta_w \tan\beta_{w0}\Delta\tau_3) \tag{28}$$

where the operator ± value depends respectively on whether the rope is lang lay or regular lay. Then, the axial strain of the double-helix wire can be derived by

$$\xi_4 = \frac{\sqrt{\left[(h_{s0})^2 + (l_{s0})^2\right](1+\xi_3)^2 + (l_w)^2}}{\sqrt{(h_{s0})^2 + (l_{s0})^2 + (l_{w0})^2}} - 1 \tag{29}$$

In fact, it is convenient to consider the Poisson effect since the axial strain is uniform in frictionless condition. Considering the variation of the spiral radius of the single-helix wire, Eq. (24) will be written as

$$l_s' = r_s'(\theta + k_t h_{s0}) \tag{30}$$

where

$$r_s' = R_1(1-\nu\xi_1) + 2R_2(1-\nu\xi_2) + 2R_4(1-\nu\xi_4) + R_3(1-\nu\xi_3) \tag{31}$$

Here ξ_1 and ξ_2 represents the strain of the straight wire and the single-helix wire in the core strand respectively. The axial strain of the single-helix wire in the wound strand is now obtained by

$$\xi_3' = \frac{\sqrt{(h_s)^2 + (l_s')^2}}{\sqrt{(h_{s0})^2 + (l_{s0})^2}} - 1 \tag{32}$$

The spiral angle of the single-helix wire is given by

$$\alpha_s' = \tan^{-1}\left(\frac{h_{s0}(1+\varepsilon_t)}{r_s'(\theta + k_t h_{s0})}\right) \tag{33}$$

Here the curvature variation $\Delta\kappa_3'$ and the twist variation $\Delta\tau_3$ also have changed. We denote them by $(\Delta\kappa_3')'$ and $(\Delta\tau_3)'$ now respectively and they can still be calculated from similar equations as Eq. (19) by using the angle α_s'.

It should be noted that ξ_3 and ξ_4 on the right end of Eq. (31) are obtained from Eq. (26) and Eq. (29) by ignoring the Poisson effect (ξ_2 can be got from a similar equation as Eq. (26)). The main reason for this simplification is that $\nu\xi_i$ ($i = 1,\ldots,4$) considered in present work is a minor term compared to the value of 1 in Eq. (31).

Considering the Poisson effect, the circumferential length of the double-helix centerline after deformation can be rewritten as

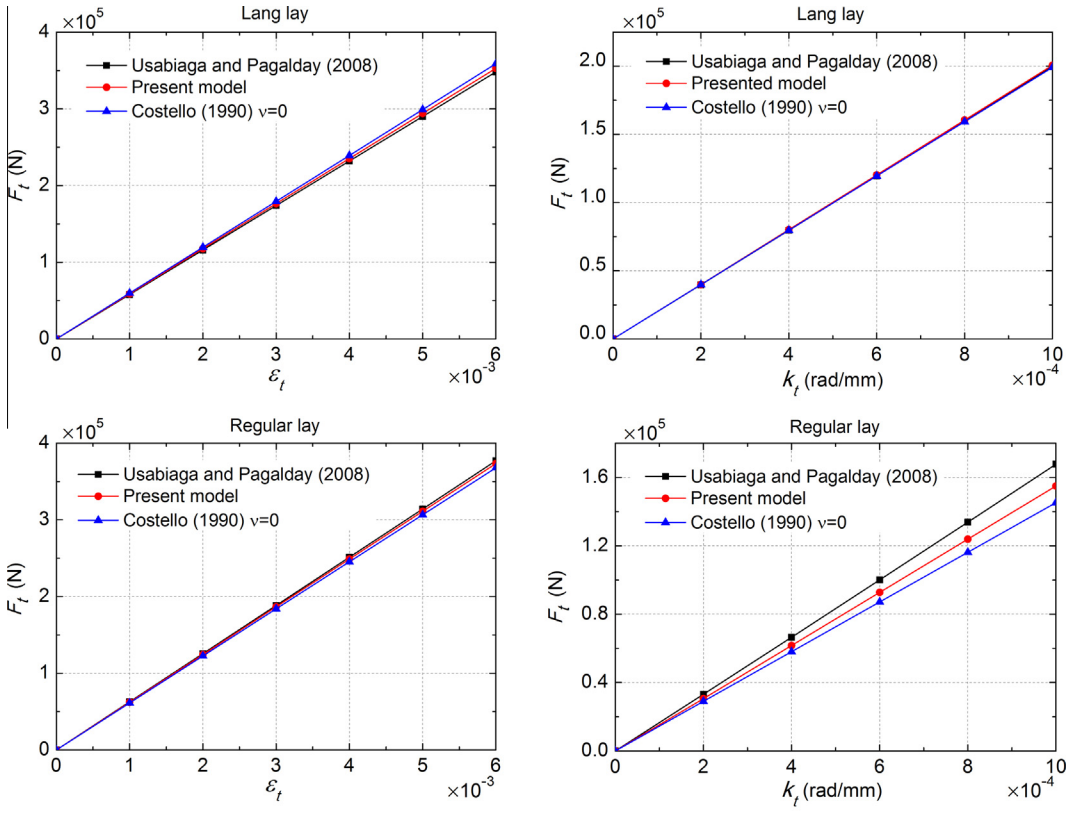

(a) $\varepsilon_t = 0.001, \ldots, 0.006,\ k_t = 0$ (b) $\varepsilon_t = 0.0001,\ k_t = 0, \ldots, 0.001\,\text{rad/mm}$

Fig. 6. Axial force prediction for lang and regular lay ropes in different loading conditions.

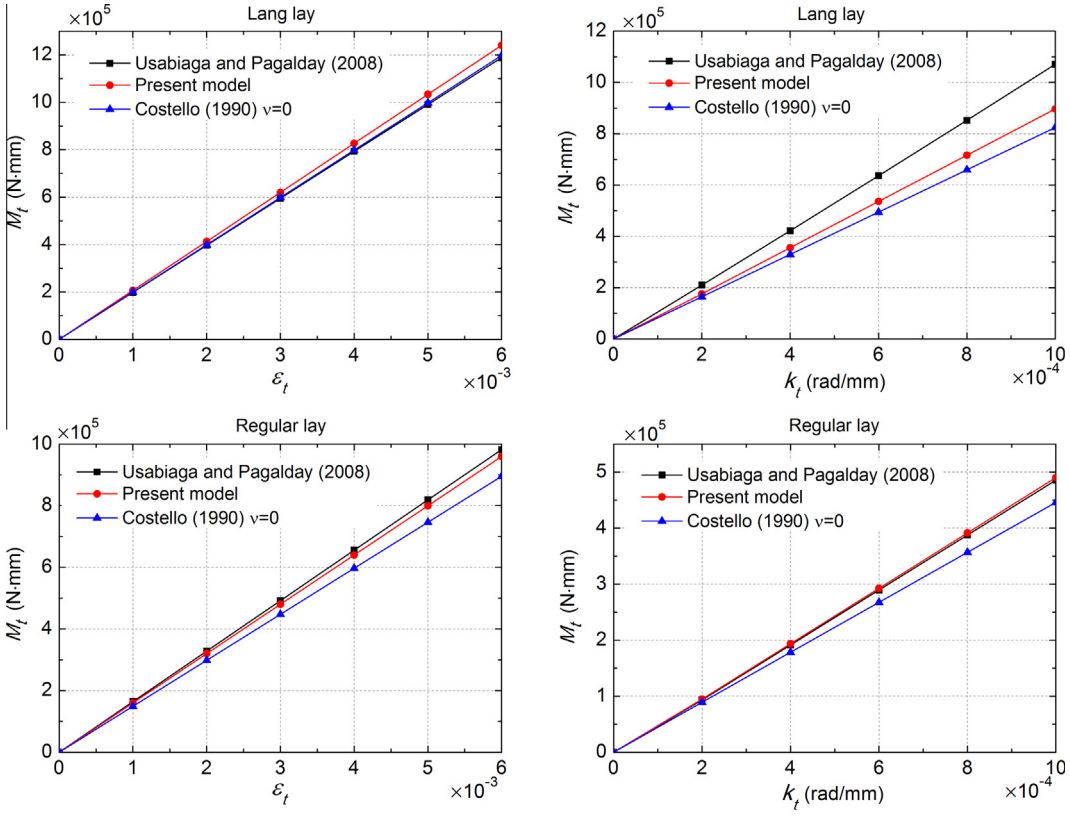

Fig. 7. Axial torque prediction for lang and regular lay ropes in different loading conditions.

Table 2
Stiffness of the lang and regular lay ropes.

	Lang lay	Regular lay
C_{11} (N)	5.879×10^7	6.219×10^7
C_{12} (N mm)	2.068×10^8	1.602×10^8
C_{21} (N mm)	2.007×10^8	1.550×10^8
C_{22} (N mm^2)	8.968×10^8	4.984×10^8
$\frac{C_{12}-C_{21}}{C_{12}}$ (%)	2.95	3.25

$$l'_w = r'_w(\theta_w \pm r_{w0}\theta_w \tan\beta_{w0}\Delta\tau_3) \tag{34}$$

where

$$r'_w = R_3(1 - v\xi_3) + R_4(1 - v\xi_4) \tag{35}$$

and ξ_3 and ξ_4 are given by Eqs. (26) and (29) respectively. Then the axial strain of the double-helix wire is now calculated by

$$\xi'_4 = \frac{\sqrt{\left[(h_{s0})^2 + (l_{s0})^2\right](1+\xi'_3)^2 + (l'_w)^2}}{\sqrt{(h_{s0})^2 + (l_{s0})^2 + (l_{w0})^2}} - 1 \tag{36}$$

4. Axial tension and torque of a rope

When the axial strain along a wire is known, the axial force in the wire can be described by

$$T = EA\xi \tag{37}$$

where A is the area of the cross section, i.e. $A = \pi R^2$.

Shear forces N and N' can be directly calculated from Eq. (13d) and Eq. (13e) if we neglect K and K' due to the frictionless assumption, just as the work of Costello (1990). The rest of non-zero distributed loads X, Y and Z may be also calculated from Eqs. (13a)–(13c) respectively, which can be interpreted as contact forces between adjacent wires.

The contribution of a particular wire to the global tension and torque of the rope is made by projecting the local forces and moments of a wire cross section in the *principal torsion-flexure axes* $\{\boldsymbol{x}, \boldsymbol{y}, \boldsymbol{z}\}$ to the global Cartesian coordinate system $\{\boldsymbol{e}_X, \boldsymbol{e}_Y, \boldsymbol{e}_Z\}$ (Usabiaga and Pagalday, 2008). That is

$$F_i = (N_i \cdot \boldsymbol{x} + N'_i \cdot \boldsymbol{y} + T_i \cdot \boldsymbol{z}) \cdot \boldsymbol{e}_Z \tag{38}$$

$$M_i = (\boldsymbol{\rho} \times N_i \cdot \boldsymbol{x} + \boldsymbol{\rho} \times N'_i \cdot \boldsymbol{y} + \boldsymbol{\rho} \times T_i \cdot \boldsymbol{z} + G_i \cdot \boldsymbol{x} + G'_i \cdot \boldsymbol{y} + H_i \cdot \boldsymbol{z}) \cdot \boldsymbol{e}_Z \tag{39}$$

where $\boldsymbol{\rho}$ is the vector from the considered wire centroid to its nearest point on the rope central axis.

Then the total response of the rope can be computed by

$$F_t = \sum_1^{n_t} F_i \tag{40a}$$

and

$$M_t = \sum_1^{n_t} M_i \tag{40b}$$

where n_t is total number of the wires and F_t and M_t are the total tensile force and torque of the rope respectively.

When subjected to external load, the rope shows a coupling of tensile and torsional response. In the linear case, it can be expressed as

$$\begin{Bmatrix} F_t \\ M_t \end{Bmatrix} = \begin{bmatrix} C_{11} & C_{12} \\ C_{21} & C_{22} \end{bmatrix} \begin{Bmatrix} \varepsilon_t \\ k_t \end{Bmatrix} \tag{41}$$

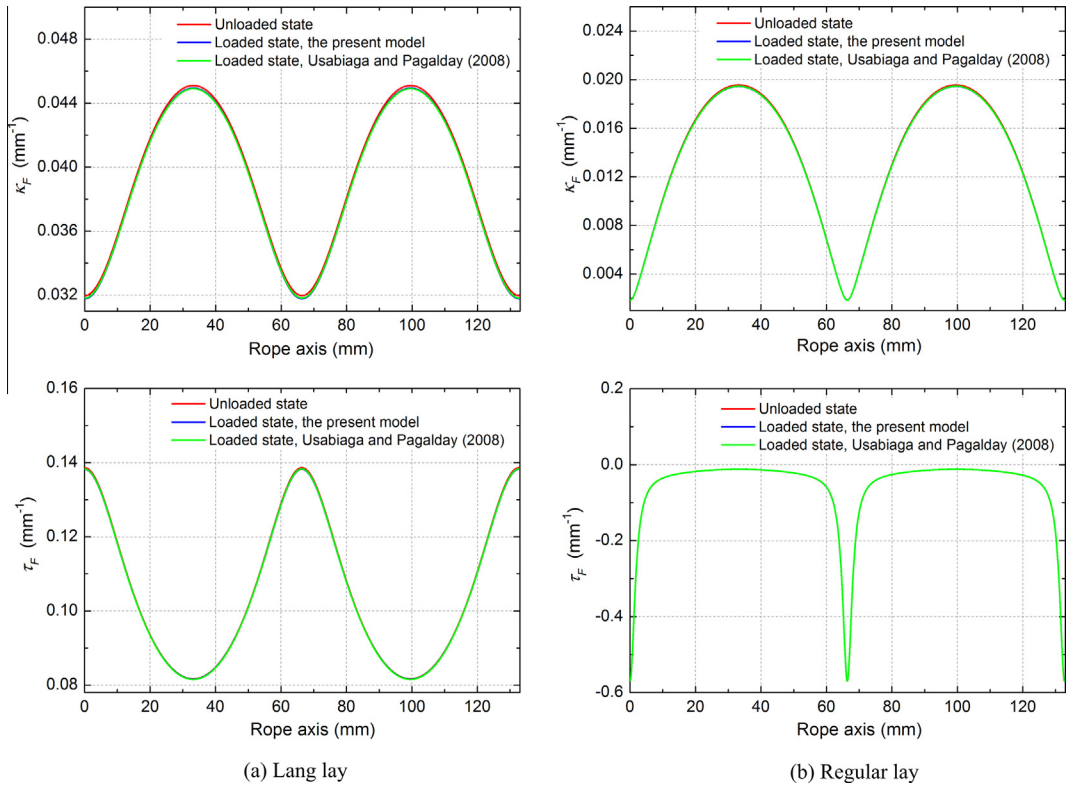

Fig. 8. Curvature and torsion defined by the Frenet–Serret frame for the double-helix wire before deformation and for $\varepsilon_t = 0.003$ and $k_t = 0$.

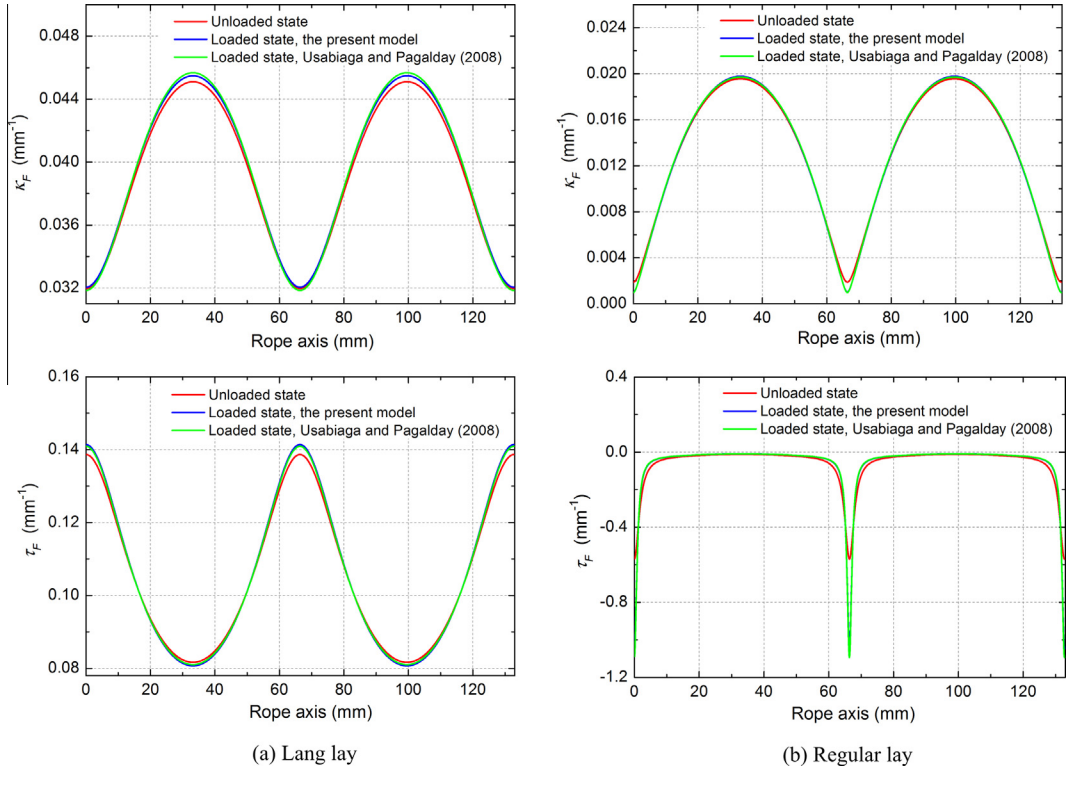

Fig. 9. Curvature and torsion defined by the Frenet–Serret frame for the double-helix wire before deformation and for $\varepsilon_t = 0.0001$ and $k_t = 0.001$ rad/mm.

The four parameters C_{11}, C_{12}, C_{21} and C_{22} denote the global stiffness of the rope. As discussed by Elata et al. (2004), and Usabiaga and Pagalday (2008), the stiffness matrix must be symmetric according to the reciprocity theorem of Betti, i.e. $C_{12} = C_{21}$. This is a verification of the consistency of a wire rope model and our model will be verified in Section 5.

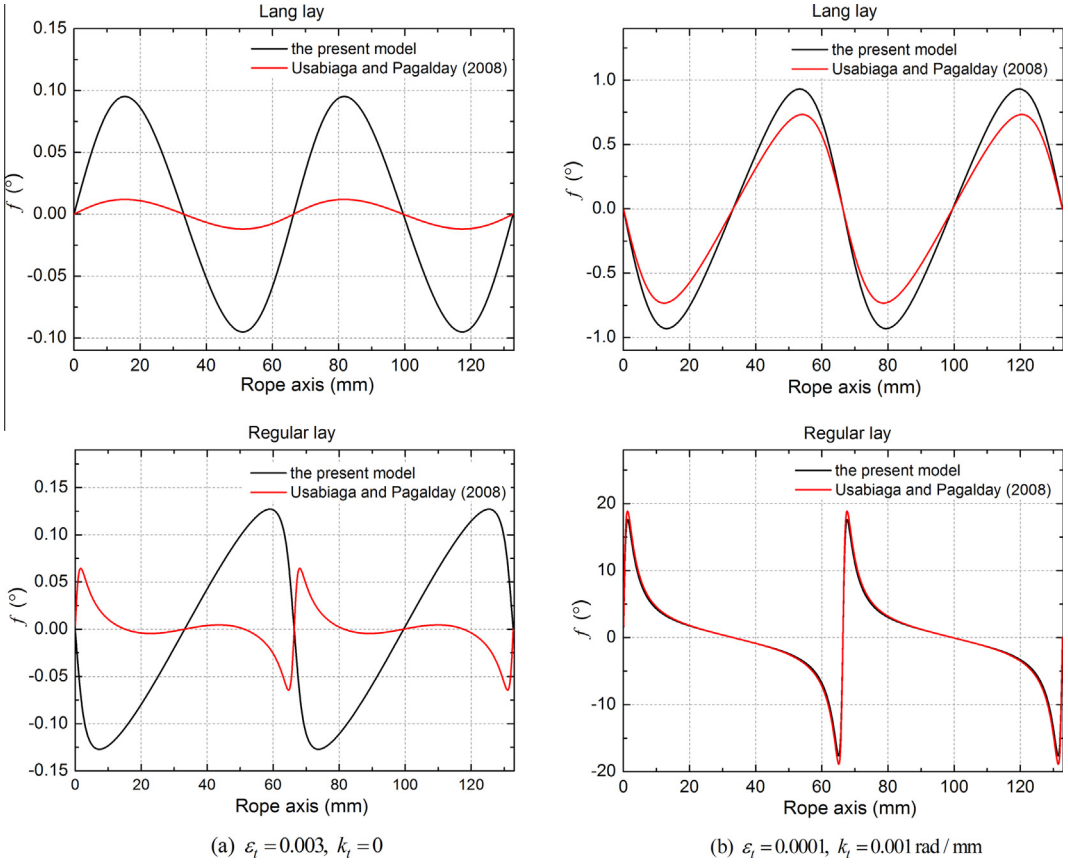

Fig. 10. The angle f of the double-helix wire in different loading conditions.

5. Results and discussion

A 7 × 7 multi-strand wire rope (IWRC) is chosen to illustrate the model in this paper, both for regular lay and lang lay constructions. Table 1 lists the main geometrical parameters of the considered rope (Usabiaga and Pagalday, 2008). For all the wires in the rope, an elastic constitutive law with elastic modulus E of 200 GPa and Poisson ratio v of 0.3 is considered.

5.1. Global rope response

Figs. 6 and 7 illustrate global response of ropes in different loading conditions. Results of Costello (1990) and Usabiaga and Pagalday (2008) are displayed as well. As the present model and the model of Usabiaga and Pagalday (2008) ignore the Poisson effect, the results of Costello' model considering $v = 0$ are chosen for rigorous comparison. Usabiaga and Pagalday (2008) have discussed that it doesn't show significant difference between $v = 0$ and $v = 0.3$ for Costello' model.

Generally the present model shows a similar performance with the homogenized model of Costello (1990). The result of the present model is a little bigger than that of Costello (1990) for the axial torque predicted for regular lay rope in Fig. 7, but not more than 10%. However, the result of Usabiaga and Pagalday (2008) is much higher than the other two models for the force predicted of regular lay rope in Fig. 6(b) and the torque predicted of lang lay rope in Fig. 7(b) (up to 25%), which generates a much bigger C_{21} for the regular lay rope and a much bigger C_{22} for the lang lay rope. This may be due to the infinite friction assumption made by the authors. As relative movements between adjacent wires are totally prevented, the rope may tend to behave like a simple complete rod, which leads to some degree of stiffer reaction to the external load.

Table 2 lists all calculated rope stiffness constants for the characterized lang and regular lay ropes. Generally, the axial torque of a lang lay rope is larger than that of a regular lay rope, especially when the rope is subjected to torsion load. That is, both C_{21} and C_{22} for lang lay are bigger than those for regular lay. However, there is no significant difference between the C_{11} for lang and regular lay ropes, indicating a similar axial force when the rope is subjected to global tension. As is previously discussed in this paper, a model should be fully compliant with the Betti reciprocity theorem. The results in Table 2 verify the symmetry of the stiffness matrix in Eq. (41), i.e. the difference between C_{12} and C_{21} is negligible for lang and regular lay ropes.

Another point that should be taken into account is the rope level equilibrium balance. As independent equilibrium of an individual wire has been discussed in Section 3.3, one need to verify whether the present model leads to a good global equilibrium. That is, the resultant tensile force and torque of any cross section of the rope axis should be equal to the values generated at the ends of the rope. Every loading and rope configuration case in Figs. 6 and 7 has been examined. Results show that the deviation of resultant tensile forces and torques is usually not more than 1%, and the deviation of resultant torque for regular lay under torsion load is a little higher but still lower than 3%. Thus, a consistent global equilibrium has been verified as well.

Reedlunn et al. (2013) found that the lubrication (friction) does not have appreciable effect on the rope stiffness constant C_{11} of shape memory alloy cables by experiments, which is coincident with the force results predicted by the models with different friction assumptions in Fig. 6(a). Velinsky et al. (1984) and Elata et al. (2004) compared their theoretical prediction with experiment results and found that the tension–elongation stiffness C_{11} was larger than the measured values (up to 10–20%). This may

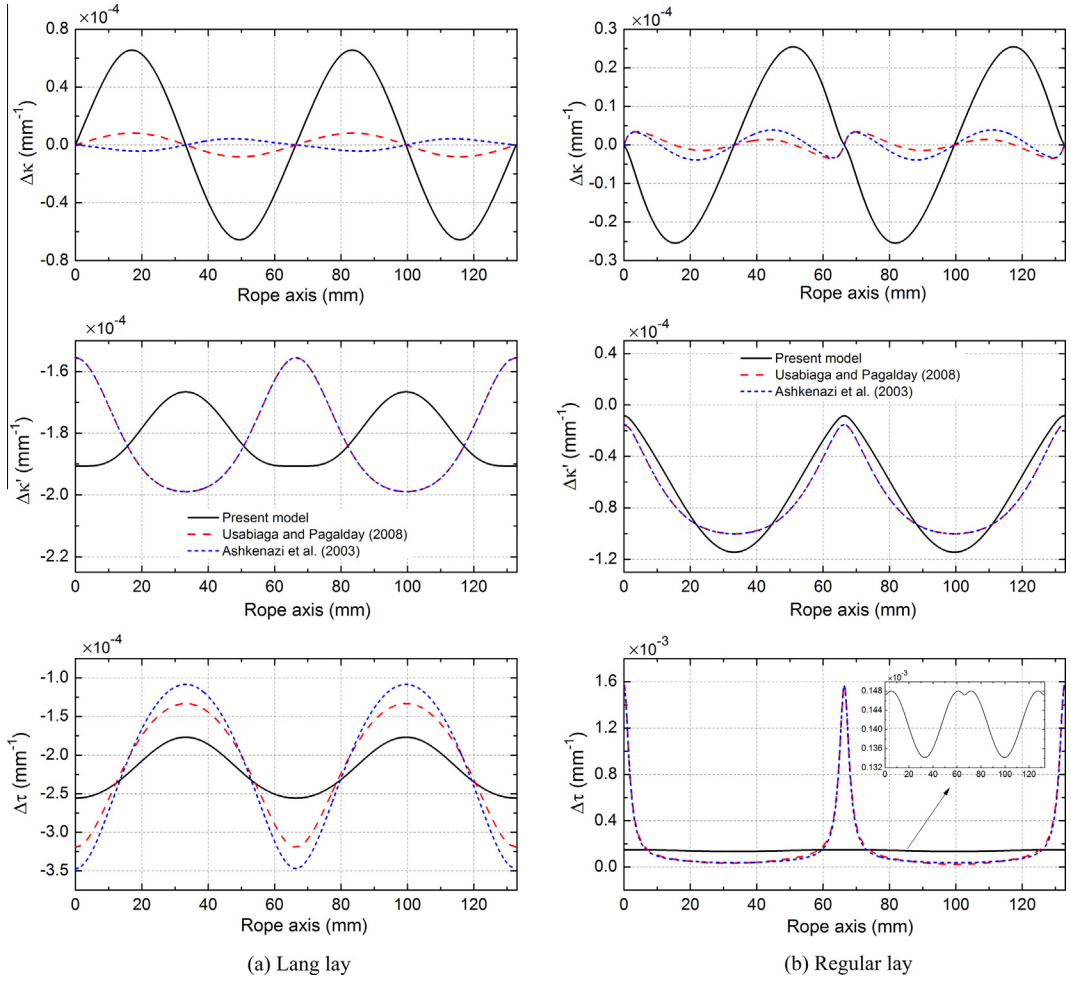

Fig. 11. $\Delta\kappa$, $\Delta\kappa$' and $\Delta\tau$ calculated from the present model and the kinematics of Usabiaga and Pagalday (2008) and Ashkenazi et al. (2003) for $\varepsilon_t = 0.003$ and $k_t = 0$.

be due to the neglection of the contact deformation between the wires and the outer strands tend to settle inside the rope core during the experiment process (Costello, 1990). These situations are not included in the present work as well. Thus, our model will give a basic prediction of the rope global stiffness.

5.2. Bending and twisting along double-helix wires

The values of the curvature κ_F, the torsion τ_F and the angle f are calculated first as curvatures and twist of wires are computed from Eq. (12). Figs. 8–10 illustrate the three parameters respectively. Actually, the angle f is not calculated in the work of Usabiaga and Pagalday (2008). We get their value of f by the following equation derived from Eq. (12a):

$$f = \arcsin(\kappa/\kappa_F) \tag{42}$$

From Figs. 8 and 9, we can find that both κ_F and τ_F of the present model and the model of Usabiaga and Pagalday (2008) differ just a little with each other after deformation, even if the two models take different centerline descriptions of double-helix wires in the deformed configuration. However, the f of the present model is usually much bigger than that of Usabiaga and Pagalday (2008) except when a regular lay rope is subjected to global torsion load (Fig. 10(b)). As the present model ignores the friction, the wires are easier to slide and move in the rope, which may generate a bigger f than the infinite friction model of Usabiaga and Pagalday (2008).

Figs. 11 and 12 show the curvatures and the twist variation $\Delta\kappa$, $\Delta\kappa'$ and $\Delta\tau$ for lang lay and regular lay double-helix wires in different loading conditions. The results of the kinematics assumption proposed by Usabiaga and Pagalday (2008) and Ashkenazi et al. (2003) (which was also materialized by Usabiaga and Pagalday, 2008) for a un-lubricated rope are also given. As depicted by the figures, the approaches lead to significant difference for almost all the cases.

Firstly, from Eqs. (12a) and (16), $\Delta\kappa$ can be calculated by

$$\Delta\kappa = \kappa - \kappa_0 = \kappa_F \sin f \tag{43}$$

So a much bigger $\Delta\kappa$ is gotten when the rope is subjected to axial tension (Fig. 11), since κ_F after deformation are nearly equal and f of the present model is much higher than that of Usabiaga and Pagalday (2008). This leads to more prominent bending deformation for wires in a well-lubricated rope.

Secondly the difference in $\Delta\kappa'$ of the models is analyzed. As we can see in Fig. 10, the f always has a very small value (lower than 1°), except for the regular lay wires under global torsion load (up to 17.5° but in a narrow region). Therefore the calculation of $\Delta\kappa'$ can be simplified as

$$\Delta\kappa' = \kappa_F \cos f - \kappa_{F0} \approx \kappa_F - \kappa_{F0} \tag{44}$$

Then the different values of $\Delta\kappa'$ calculated from the models are related to the different centerline descriptions of wires taken by the authors after deformation. The present model takes the centerline descriptions improved from Elata et al. (2004) while other

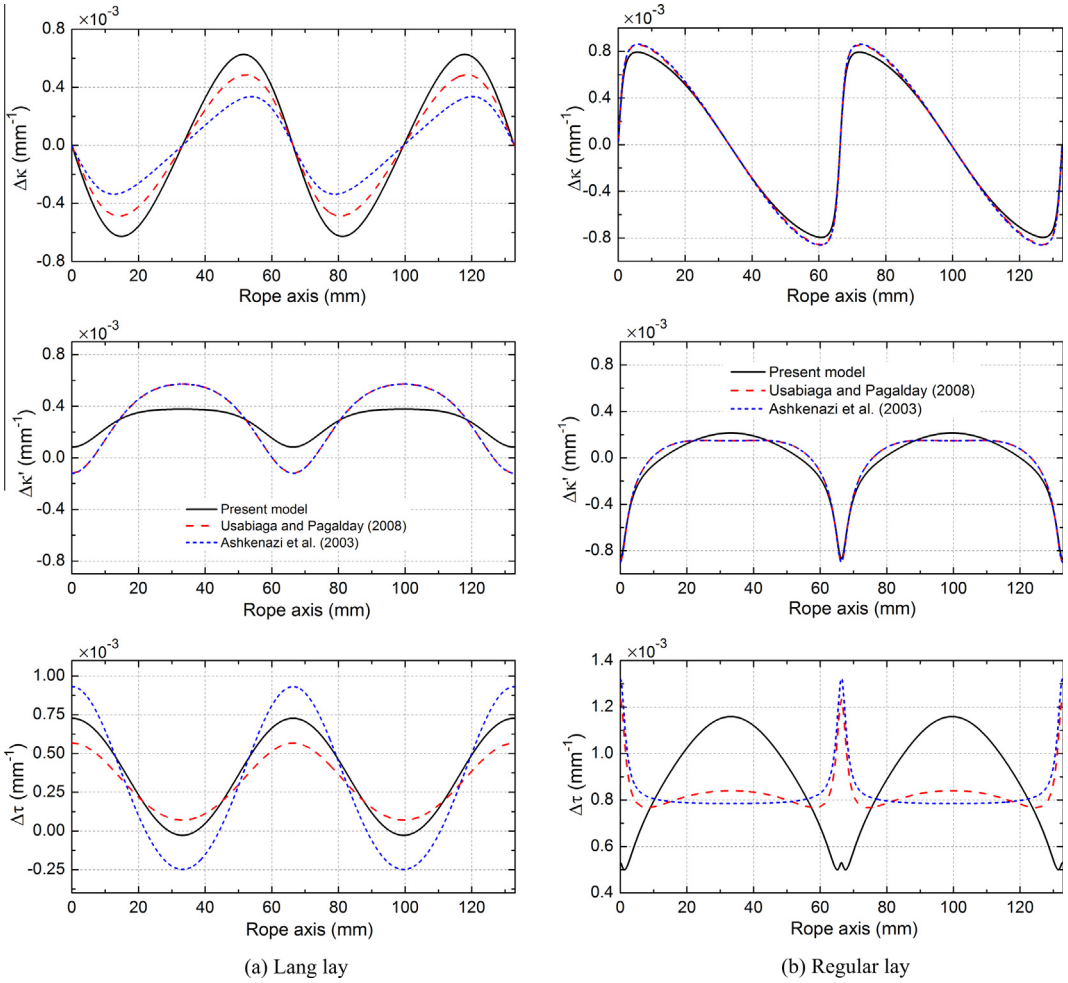

Fig. 12. $\Delta\kappa$, $\Delta\kappa'$ and $\Delta\tau$ calculated from the present model and the kinematics of Usabiaga and Pagalday (2008) and Ashkenazi et al. (2003) for $\varepsilon_t = 0.0001$ and $k_t = 0.001$ rad/mm.

Table 3
Axial strain of the wires in lang and regular lay ropes.

Rope configuration	Model	$\varepsilon_t = 0.001,\ k_t = 0$ ($\times 10^{-3}$)			$\varepsilon_t = 0,\ k_t = 0.001$ rad/mm ($\times 10^{-3}$)		
		ξ_2	ξ_3	ξ_4	ξ_2	ξ_3	ξ_4
Lang lay	Present model ($\nu = 0$)	0.894	0.899	0.816	1.186	3.148	3.491
	Present model ($\nu = 0.3$)	0.864	0.872	0.773	1.167	3.086	3.364
	Costello's model ($\nu = 0.3$)	0.864	0.873	0.775	1.162	3.048	3.337
Regular lay	Present model ($\nu = 0$)	0.894	0.899	0.853	1.186	3.148	2.357
	Present model ($\nu = 0.3$)	0.864	0.872	0.807	1.167	3.096	2.248
	Costello's model ($\nu = 0.3$)	0.864	0.872	0.809	1.162	3.058	2.205

authors follow the descriptions of Usabiaga and Pagalday (2008), so the values of $\Delta\kappa'$ are nearly the same between the work of Ashkenazi et al. (2003) and Usabiaga and Pagalday (2008), which both differ from the present model.

Finally the most significant difference occurs in $\Delta\tau$. When the rope is subjected to global tensile load (Fig. 11), the peak value of $\Delta\tau$ of the present model is much smaller than other models. The difference can be up to 10 times, which indicates much slighter torsion deformation of the ropes. For regular lay configuration (Figs. 11(b) and 12(b)), the values from the work of Ashkenazi et al. (2003) and Usabiaga and Pagalday (2008) vary severely near the ends of a variation period, which indicates that the torsion stress also changes greatly when the wire is spiral to its innermost position in the rope. This may be due to the infinite friction kinematics applied on wires. As all relative movements between adjacent wires are prevented, the significant geometric variation (see τ_F in Figs. 8(b) and 9(b)) near the ends of a variation period may be attached to the local deformation of the wires, when load is imposed to the rope. However, the present work is based on frictionless hypothesis, so the wires are free to slide and the sticking effect does not exist. This may be the reason why the present model generates more smooth curves of $\Delta\tau$.

Overall we can conclude that: in contrast to the model of Usabiaga and Pagalday (2008) and Ashkenazi et al. (2003), the present model generates more prominent bending deformation and much slighter torsion deformation when the rope is subjected

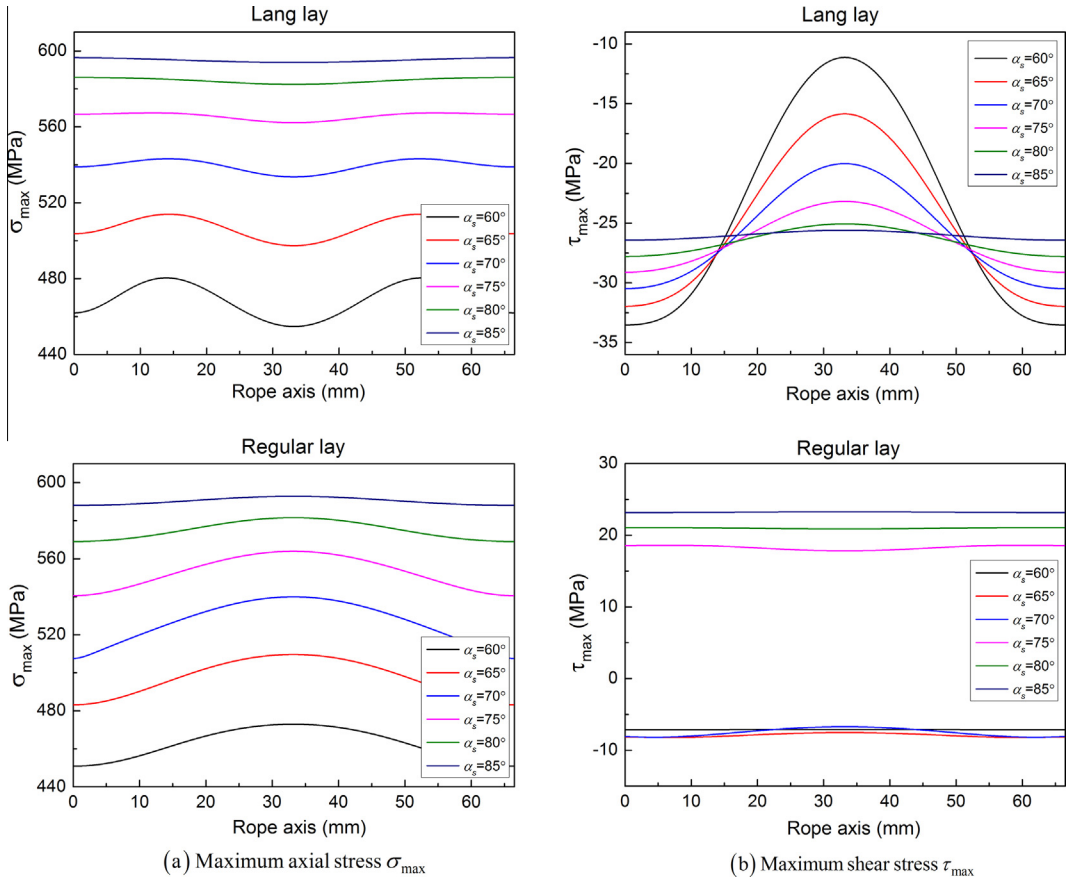

Fig. 13. Variations of the maximum axial stress and the maximum shear stress in a double-helix wire with its corresponding single-helix laying angle α_s, where $\beta_w = 75°$, $r_s = 10.0$ mm, $r_w = 3.0$ mm and $\varepsilon_t = 0.003$, $k_t = 0$.

to axial tension and more smooth variation of torsion deformation when the rope is subjected to axial torque. All these are mainly due to the different friction assumption made by the authors to their models, as analyzed above.

5.3. Stress analysis in the wires

Now we analyze the stresses in the wires caused by axial tension, torsion, and bending. When a rope is subjected to axial tension and torsion, the internal forces and moments acting on its wires can be determined by Eqs. (14) and (37). The axial stresses in each wire are mainly induced by its axial force T and bending moments G and G', while the shear stresses result mainly from the torque H. The axial stress in the center of a wire cross-section is

$$\sigma_c = \frac{T}{A} = E\xi \tag{45}$$

The maximum axial stress and the maximum shear stress in a wire can be calculated by

$$\sigma_{\max} = \sigma_c + \frac{4\sqrt{G^2 + G'^2}}{\pi R^3} \tag{46}$$

$$\tau_{\max} = \frac{2H}{\pi R^3} \tag{47}$$

respectively.

The axial stress σ_c along a wire is uniform in frictionless condition and changes linearly with the axial strain ξ. Table 3 gives the axial strain of the wires, with the Poisson effect into consideration or not. When taking $\nu = 0.3$ into computation, the results of the present model are very close to those of Costello (1990). In global tension load, the axial strain of a double-helix wire in a lang lay rope is a little lower than that in a regular lay one, while it is much bigger when the rope is subjected to axial torsion. Regarding to the Poisson effect, one can see that the values considering the radial contraction in the wire diameter are just a little lower than those ignoring it.

Figs. 13 and 14 illustrate the variations of $\sigma_{\max}$ and $\tau_{\max}$ with the single-helix laying angle α_s and the double-helix laying angle β_w when the rope is subjected to axial tension respectively. It can be seen that $\sigma_{\max}$ in the double-helix wire increases monotonously when α_s or β_w changes from 60° to 85°. The variation of $\tau_{\max}$ is complicated, as its direction and its peak value or average value along the rope axis vary simultaneously with the change of the two angles. The lang lay and the regular lay wires show a very similar stress level of $\sigma_{\max}$, while the level of $\tau_{\max}$ for regular lay is usually a little lower than that for lang lay.

To be noted, the magnitude of $\tau_{\max}$ is much lower than that of $\sigma_{\max}$. It indicates that the torsion stress in a double-helix wire can be neglected when the rope is subjected to axial tension. It should also be noted is that all the stress curves become flat when α_s or β_w is close to 90°. The reason is that when both α_s and β_w are equal to 90°, the double-helix wire turns into a totally straight wire, in which the stresses along the wire are uniform when it is subjected to axial tension.

The stresses in the wires are not analyzed here when the rope is subjected to axial torque, as most wire ropes in practical cases are used to transmit the big tensile force, and relatively the axial torsion is not prominent.

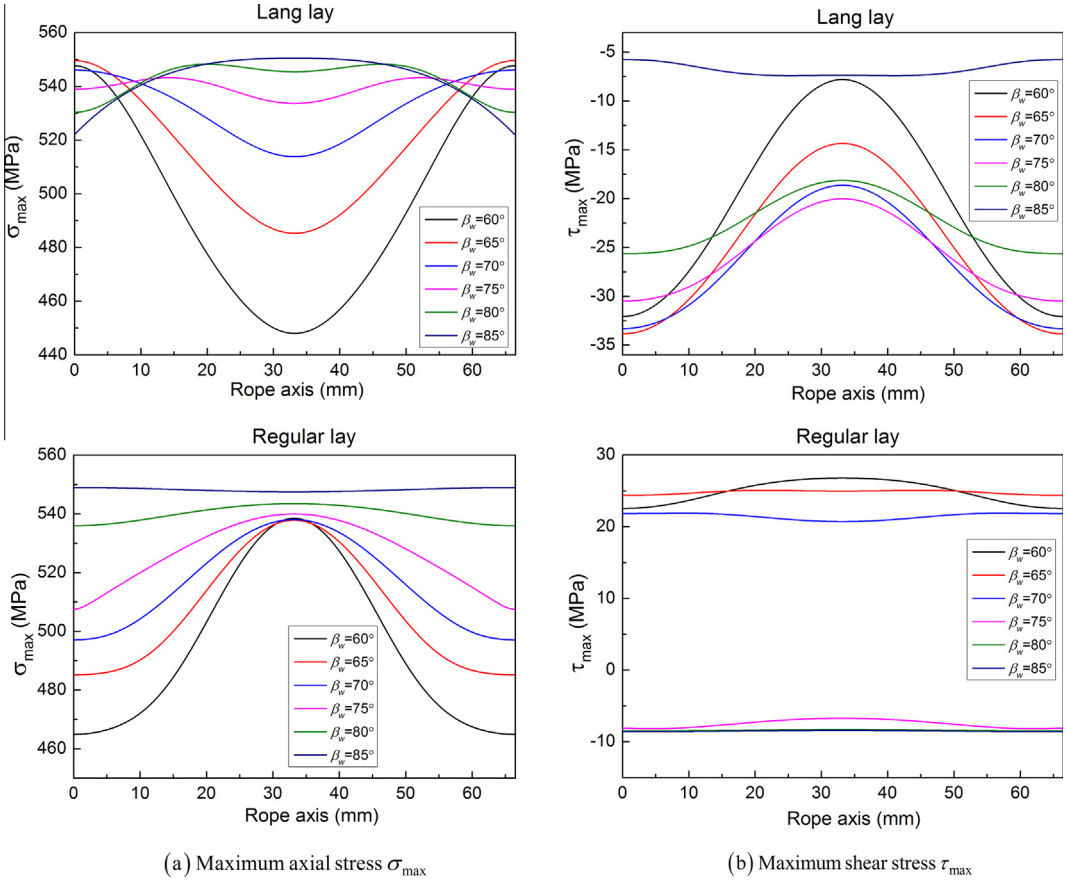

(a) Maximum axial stress σ_{max} (b) Maximum shear stress τ_{max}

Fig. 14. Variations of the maximum axial stress and the maximum shear stress in a double-helix wire with double-helix laying angle β_w, where $\alpha_s = 70^\circ$, $r_s = 10.0$ mm, $r_w = 3.0$ mm and $\varepsilon_t = 0.003$, $k_t = 0$.

6. Conclusions

A new wire rope model based on frictionless assumption and Love's general thin rod theory is proposed. Comparing with previous approaches, this model fully considers the double-helix configuration in multi-strand wire ropes. Specifically, local bending and torsion deformation parameters of each wire are completely computed, instead of assuming a fibrous response of each wire or homogenizing a wound strand as being a wire. The use of the angle "f" generates concise equations to compute the curvatures and the twist from the equilibrium equations and helps to understand and explain the related results. The present model is convinced of a correct estimation of rope global stiffness. And the consistency of the model has been examined by the invariability of resultant tensile force and torque along the axis of the rope and by the symmetry of the stiffness matrix of the rope.

This model also incorporates some procedures to get the axial strain along wires. Results show that it does not lead to distinct difference, taking the Poisson effect into account or not, and the axial strain contributes most of global force and torque of the rope (Usabiaga and Pagalday, 2008). It indicates that the Poisson effect may not have significant influence on the rope global behavior.

The local curvatures and twist along double-helix wires have shown much difference between the present model and other models, due to different friction assumptions made to the wires. As most of ropes are well-lubricated to prevent the frictional contact and wear damage of the wires, our frictionless model may be closer to the actual situation and have a broader application, in contrast to the infinite friction model of Usabiaga and Pagalday (2008).

Concerning the local stresses, the lang lay and regular lay wires show similar stress levels and the torsion stress of a double-helix wire can be neglected, when the rope is subjected to axial tension. The maximum axial stress of a double-helix wire is positively related to the double-helix laying angle and its corresponding single-helix laying angle. The stresses in the wires are critically relevant to rope endurance analysis when rope is under fluctuating loads and the analysis of stresses changing with different geometric parameters will help researchers to design optimal rope structures with a more uniform load distribution between the wires. What's more, the proposed model can provide integrated estimations of inter-wire interactions (like contact forces) from the equilibrium equations of each wire, which is useful to predict the fretting fatigue property at the wire level.

The current rigorous description of the procedure to compute Love's (1944) kinematic parameters can be easily extended to the wires of higher helix levels. However, ignoring the Poisson effect and contact deformation may have some influence on the local stresses. Contact deformation has been analyzed by Argatov (2011) and Páczelt and Beleznai (2011) for a straight strand, which may be expanded to double-helix wires in the future. In addition, all the local deformation results need to be verified by careful experiments and the finite element method, which can provide local strain and stress information of the wires, and more practical cases with a finite friction coefficient and Poisson radial contraction should be taken into account.

Acknowledgments

The work is supported by the Nature Science Foundation of China (Grants Nos. 11472287, 11132011 and 11202221), the National Basic Research Program of China (Grants No. 2012CB937500), the CAS Science and Technology Innovation Program (Grants No. CXJJ-14-Z66), and the CAS/SAFEA International Partnership Program for Creative Research Teams.

References

Argatov, I., 2011. Response of a wire rope strand to axial and torsional loads: asymptotic modeling of the effect of interwire contact deformations. Int. J. Solids Struct. 48, 1413–1423.

Ashkenazi, R., Weiss, M.P., Elata, D., 2003. Torsion and bending stresses in wires of non-rotating tower crane ropes. In: OIPEEC Technical Meeting: Experiences with Ropes, Lenzburg, Suiza, pp. 77–99.

Blouin, F., Cardou, A., 1989. A study of helically reinforced cylinders under axially symmetric loads and application to strand mathematical modelling. Int. J. Solids Struct. 25 (2), 189–200.

Cardou, A., Jolicoeur, C., 1997. Mechanical models of helical strands. Appl. Mech. Rev. 50, 1–14.

Costello, G.A., 1990. Theory of Wire Rope. Springer-Verlag, New York.

Costello, G.A., Philips, J.W., 1976. Effective modulus of twisted wire cables. J. Eng. Mech. Div., ASCE 102, 171–181.

Elata, D., Ashkenazi, R., Weiss, M., 2004. The mechanical behaviour of a wire rope with an independent wire rope core. Int. J. Solids Struct. 41, 1157–1172.

Feyrer, K., 2006. Wire Ropes: Tension Endurance Reliability, first ed. Springer.

Ghoreishi, S.R., Cartraud, P., Davies, P., Messager, T., 2007a. Analytical modeling of synthetic fiber ropes subjected to axial loads. Part I: A new continuum model for multilayered fibrous structures. Int. J. Solids Struct. 44 (9), 2924–2942.

Ghoreishi, S.R., Cartraud, P., Davies, P., Messager, T., 2007b. Analytical modeling of synthetic fiber ropes. Part II: A linear elastic model for 1 + 6 fibrous structures. Int. J. Solids Struct. 44 (9), 2943–2960.

Ghoreishi, S.R., Messager, T., Cartraud, P., Davies, P., 2007c. Validity and limitations of linear analytical models for steel wire strand under axial loading, using a 3D FE model. Int. J. Mech. Sci. 49 (11), 1251–1261.

Hobbs, R.E., Raoof, M., 1982. Interwire slippage and fatigue prediction in stranded cables for TLP tethers. Behaviour of Offshore Structures, vol. 2. Hemisphere publishing/McGraw-Hill, New York, pp. 77–99.

Hruska, F.H., 1952a. Radial forces in wire ropes. Wire Wire Prod. 27, 459–463.

Hruska, F.H., 1952b. Tangential forces in wire ropes. Wire Wire Prod. 28, 459–463.

Inagaki, K., Ekh, J., Zahrai, S., 2007. Mechanical analysis of second order helical structure in electrical cable. Int. J. Solids Struct. 44 (5), 1657–1679.

Jolicoeur, C., 1997. Comparative study of two semicontinuous models for wire strand analysis. J. Eng. Mech. 123 (8), 792–799.

Jolicoeur, C., Cardou, A., 1991. A numerical comparison of current mathematical models of twisted wire cables under axisymmetric loads. J. Energy Res. Technol. 113, 241–249.

Knapp, R.H., 1979. Derivation of a new stiffness matrix for helically armoured cables considering tension and torsion. Int. J. Numer. Methods Eng. 14, 515–529.

Kumar, K., Cochran, J.J.E., 1987. Closed-form analysis for elastic deformations of multilayered strands. J. Appl. Mech. 54 (4), 898–903.

Lanteigne, J., 1985. Theoretical estimation of the response of helically armored cables to tension, torsion, and bending. J. Appl. Mech. 52, 423–432.

LeClair, R., Costello, G.A., 1988. Axial, bending and torsional loading of a strand with friction. J. Offshore Mech. Arct. Eng. 110, 38–42.

Lee, W.K., 1991. An insight into wire rope geometry. Int. J. Solids Struct. 28 (4), 471–490.

Love, A.E.H., 1944. A Treatise on the Mathematical Theory of Elasticity. Dover Publications, New York (chapters 18 and 19).

Páczelt, I., Beleznai, R., 2011. Nonlinear contact-theory for analysis of wire rope strand using high-order approximation in the FEM. Comput. Struct. 89, 1004–1025.

Phillips, J.W., Costello, G.A., 1985. Analysis of wire ropes with internal wire rope cores. J. Appl. Mech. 52, 510–516.

Raoof, M., 1983. Interwire Contact Forces and the Static, Hysteretic and Fatigue Properties of Multi-Layer Structural Strands (Ph.D. thesis). Imperial Collage of Science and Technology, London, UK.

Raoof, M., Kraincanic, I., 1994. Critical examination of various approaches used for analysing helical cables. J. Strain Anal. Eng. Des. 29 (1), 43–55.

Reedlunn, B., Daly, S., Shaw, J., 2013. Superelastic shape memory alloy cables. Part I: Isothermal tension experiments. Int. J. Solids Struct. 50, 3009–3026.

Spak, K., Agnes, G., Inman, D., 2013. Cable modeling and internal damping developments. Appl. Mech. Rev. 65, 010801–010818.

Stanova, E., Fedorko, G., Fabian, M., Kmet, S., 2011a. Computer modelling of wire strands and ropes. Part I: Theory and computer implementation. Adv. Eng. Software 42, 305–315.

Stanova, E., Fedorko, G., Fabian, M., Kmet, S., 2011b. Computer modelling of wire strands and ropes. Part II: Finite element-based applications. Adv. Eng. Software 42, 322–331.

Usabiaga, H., Pagalday, J.M., 2008. Analytical procedure for modeling recursively and wire by wire stranded ropes subjected to traction and torsion loads. Int. J. Solids Struct. 45, 5503–5520.

Utting, W.S., Jones, N., 1987a. The response of wire rope strands to axial tensile loads. Part I: Experimental results and theoretical predictions. Int. J. Mech. Sci. 29 (9), 605–619.

Utting, W.S., Jones, N., 1987b. The response of wire rope strands to axial tensile loads. Part II: Comparison of experimental results and theoretical predictions. Int. J. Mech. Sci. 29 (9), 621–636.

Velinsky, S.A., 1981. Analysis of Wire Ropes with Complex Cross Sections (Ph.D. thesis). Department of Theoretical and Applied Mechanics, University of Illinois at Urbana-Champaign, 87.

Velinsky, S.A., Andewn, G., Costello, G., 1984. Wire rope with complex cross sections. J. Eng. Mech. Div., ASCE 110 (3), 380–391.